ADVANCED ELECTRONIC MATERIALS Open Access
www.advelectronicmat.de

Check for updates

The Impact of Non-Monolithic Semiconductor Capacitance on Organic Electrochemical Transistors Performance and Design

*Ned E. Dreamer, Dimitrios A. Koutsouras, Morteza Hassanpour Amiri, Paschalis Gkoupidenis, and Kamal Asadi**

The existing device models for organic electrochemical transistors (OECTs) fail to provide any device design guidelines for optimized performance parameters such as transconductance that are pivotal for the applications OECTs in sensing. Moreover, the current models are based on the questionable assumption of a homogenous organic semiconductor layer, and all predict a linear behavior of the resistance with the OECT channel length. Consequently, the experimentally observed nonlinear resistance behavior in OECTs has been overlooked thus far. Here, an OECT device model is developed that accurately describes the nonlinear behavior of the OECT channel resistance and offers the first guidelines for maximizing transconductance. The model is inherently nonlinear and the nonlinearity stem from the non-monolithic capacitance of the organic semiconductor layer. Moreover, the model provides a consistent and reliable estimations for the contact resistance in OECTs. The success of the model in accurately describing and providing predictions of the OECT operation by relating the device's geometrical parameters with electrochemical parameters of the semiconductor layer paves the way toward unlocking OECT potentials in diverse applications, from biosensing to neuromorphic computing and flexible electronics.

1. Introduction

Organic electrochemical transistors (OECTs) have emerged as promising devices for a wide range of applications such as biosensors,[1] logic circuits,[2] and hardware for neuromorphic computing.[3] OECTs are thin film transistors in which an organic semiconducting channel is in direct contact with an electrolyte gate,[4,5] as schematically shown in **Figure 1a**. Contrary to a conventional transistor, the semiconductor layer in an OECT is coupled to the gate electrode via an electrolyte. The most common semiconductor used in OECTs is poly(3, 4-ethylenedioxythiophene) doped with poly(styrene sulfonate) (PEDOT:PSS), which is an ionic-semiconductor.[6–9] The application of an external bias on the electrolyte gate de-dopes the PEDOT:PSS channel via the injection of ions thereby modulating the electronic conductivity of the channel.

The first model describing current transport in an OECT channel is due to Bernards and Malliaras (BM model),[10] which considers the PEDOT:PSS channel as a conjunction of an electronic circuit with an ionic one. The electronic circuit accounts for the conductivity of the channel, whereas the ionic circuit describes the flow of ions in/out of the semiconductor channel. The ionic circuit is represented by a resistor and a capacitor that represent the flow and storage of ions, respectively. The BM model provides a prediction of the steady-state performance of OECTs and the channel current as expressed in Equation (1):[10]

$$I_D = \begin{cases} \frac{WT}{L}\mu C^* \left(\left(V_{th} - V_G\right) - \frac{V_D}{2} \right) V_D \ linear \\ \frac{WT}{2L}\mu C^* \left(V_{th} - V_D\right)^2 \ saturation \end{cases} \quad (1)$$

where W and L are the width and length of the OECT channel, respectively, T is the thickness of the PEDOT:PSS film, μ is the electronic charge carrier mobility, and C^* is the volumetric capacitance of the PEDOT:PSS layer which is assumed constant. V_G,

N. E. Dreamer, K. Asadi
Department of Physics
University of Bath
Claverton Down, Bath BA2 7AY, UK
E-mail: ka787@bath.ac.uk
D. A. Koutsouras, M. Hassanpour Amiri, P. Gkoupidenis
Max Planck Institute for Polymer Research
Ackermannweg 10, 55128 Mainz, Germany
D. A. Koutsouras
IMEC NL
Eindhoven 5656 AE, The Netherlands

The ORCID identification number(s) for the author(s) of this article can be found under https://doi.org/10.1002/aelm.202400373

© 2024 The Author(s). Advanced Electronic Materials published by Wiley-VCH GmbH. This is an open access article under the terms of the Creative Commons Attribution License, which permits use, distribution and reproduction in any medium, provided the original work is properly cited.

DOI: 10.1002/aelm.202400373

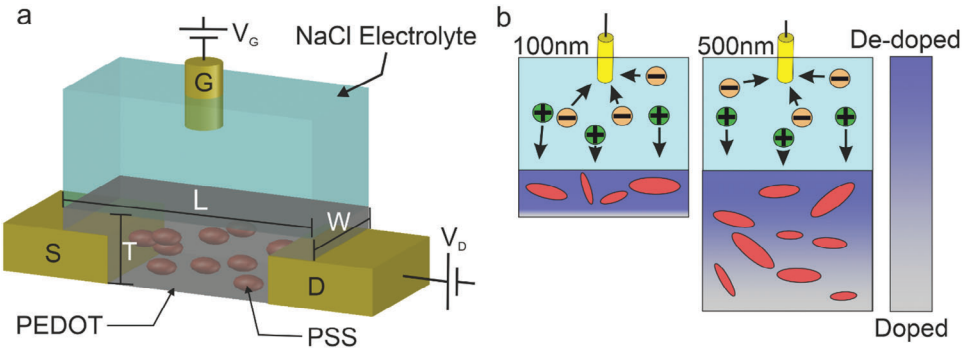

Figure 1. Device schematic and output characteristics a) 3D schematic of an OECT with PEDOT:PSS semiconductor (the grey region represent PEDOT-rich phase, whilst red ellipsoids are PSS rich phases). The channel dimensions is *W*, and *L* for width and length, respectively and *T* is PEDOT:PSS thickness. Source (S) and drain (D) are made of gold whilst gate electrode (G) is made of Ag/AgCl. Voltages V_D and V_G are applied at the drain and gate respectively. I_D is measured at the source electrode. b) Representation of de-doping process upon the application of a gate voltage and the non-monolithic de-doping across thin and thick PEDOT:PSS layers.

and V_{th} are the gate and the threshold voltages, respectively. According to this model, I_D depends on device geometry including the thickness of the PEDOT:PSS layer. The transconductance is defined as $g_m = \frac{\partial I_D}{\partial V_G}$ is usually considered as a figure of merit for an OECT, which is proportional to $\frac{WT}{L}\mu C^*$ in either of the linear or saturation regimes.

The dependence of g_m on the device geometry is not well understood and is poorly captured by current capacitive device models.[11] A recent 2D device model that takes the drift and diffusion of ions within the channel suggested that the maximum of transconductance, $g_{m(max)}$, depends on V_G. Furthermore, the V_G corresponding to $g_{m(max)}$ depended on V_D, *W*, *L*, and *T*.[12] It has been suggested that the ion concentration in the channel is not uniform, as a result of which transconductance shows linear scaling with $\frac{WT}{L}$ and saturates at higher ratios.[12]

Contact resistance, R_C, defined as the resistance between the contact and the semiconductor channel is considered as a performance limiting parameter. For example, it has been suggested that the saturation of $g_{m(max)}$ is due to the contact resistance.[11] Moreover, R_C decreases the cut-off frequency in the transient behavior of OECTs, thus negatively impacting the AC-related characteristics by adding parasitic time constants.[13] Therefore, minimizing R_C is desired for improved OECT performance, as well as for improving the performance of the corresponding OECT-based circuits.

Currently however, no analytical model exist that can be used for the derivation of contact resistance. There is limited research into contact resistance in depletion mode OECTs.[13–17] Transfer line method (TLM) has usually been employed to determine contact resistance. The TLM method considers the total resistance of an OECT, $R_{tot} = \frac{V_D}{I_D} = R_{ch} + 2R_C$, where R_{ch} is the channel resistance and R_C is the contact resistance. The factor 2 for R_C is used to account for the resistances at the source and at the drain electrodes with the semiconductor layer. For a homogeneous and uniform semiconductor R_{ch} follows Ohm's law ($= R_{sh}\frac{L}{W}$, where R_{sh} is the sheet resistance of the semiconductor layer) and scales linearly with *L*. TLM has been very effective at estimating R_C for silicon-based transistors. Thus has also been used for the estimation of R_C in OECTs.[18] While TLM has been somewhat successful, it has been inconsistent in estimating R_C often producing unphysical negative R_C values.

PEDOT:PSS exhibits a multiscale phase separation between electronically conductive PEDOT -rich and ionically conductive PSS-rich phases. The phase separation occurs from nanometer to mesoscopic length scales and depends on the polymer processing conditions.[19–21] On the other hand, TLM rests on the assumption that the semiconductor is homogeneous and uniform.[18] Therefore, the application of TLM for PEDOT:PSS OECTs is questionable because the primary condition for applicability of TLM is not satisfied.

Phase separation in PEDOT:PSS leads to a large interfacial area and the consequent formation of electrical double layer yields a large effective capacitance.[22] It has been shown that the electrochemical capacitance of PEDOT:PSS follows a linear relationship with volume, υ, in a range of υ up to $\approx 10^5$ μm^3, and the gradient gives the value for the volumetric capacitance, C^*.[23,24] The assumption of a constant C^* is valid when the entire volume of PEDOT:PSS contributes to the effective capacitance.[21] However it has been indicated that deviations from this trend may occur at higher polymer volumes, due to graded physicochemical properties such as incomplete film hydration.[23,19,25–27] Recently the assumption of the scaling of PEDOT:PSS capacitance with volume has been challenged. It has been shown that the scaling PEDOT:PSS volume is non-monotonic, where a linear trend is followed by a saturation-plateau above a critical volume, υ_c.[19] Interestingly, a correlation between the capacitance and the electroactive surface area (ESA) of the PEDOT:PSS has emerged, in which both parameters undergo saturation above the critical volume, indicating that at large volumes, PEDOT:PSS films are not fully accessible to ions of the electrolyte. Furthermore, it has been shown that the areal capacitance, C_A, defined as the ratio between the capacitance and the electroactive surface area is invariant, and that the volumetric capacitance has a validity restricted to a small volume range, where PEDOT:PSS is fully accessible to ion penetration.

The fact that the areal capacitance can be measured by cyclic voltammetry or impedance spectroscopy, prompts a new proposition to develop an OECT device model that takes C_A, and υ_c into account. However, the OECT models developed so far

© 2024 The Author(s). Advanced Electronic Materials published by Wiley-VCH GmbH

2199160x, 2024, 12, Downloaded from https://onlinelibrary.wiley.com/doi/10.1002/aelm.202400373 by MPI 355 Polymer Research, Wiley Online Library on [19/12/2024]. See the Terms and Conditions (https://onlinelibrary.wiley.com/terms-and-conditions) on Wiley Online Library for rules of use; OA articles are governed by the applicable Creative Commons License

overlook the inhomogeneity in ion distribution in the PEDOT:PSS layer, and suffer from a common shortcomings between, which is inability to offer a design criteria for the maximized transconductance or correct estimation of the contact resistance[11] as they univocally rely on the assumption of a constant volumetric capacitance,[28,29] Here, we derive an analytical model that takes critical volume and areal capacitance into account, and provides an equation describing current transport in OECTs that consistently describes devices with different channel dimensions, PEDOT:PSS thicknesses, T, at various electrolyte salt concentration. In sharp contrast, the present model produces a channel resistance that is a nonlinear function of the channel length and is able to consistently estimate the contact resistance for a large batch of devices. The non-monolithic capacitance (NMC) model provides an experimentally validated design criteria to achieve a maximum transconductance, $g_{m(max)}$, by linking the geometrical OECT parameters (T, W, and L) with the electrochemical parameters of the PEDOT:PSS (C_A, and υ_c), which can be measured independently. Our findings elucidate the mechanism of capacitive coupling in OECT devices and provide a better understanding on how to optimize the device layout for specific bioelectronics or sensing applications.

2. Results and Discussion

2.1. NMC model for OECTs

It has been experimentally demonstrated that the capacitance of the PEDOT:PSS layer with the volume υ (= WLT) is proportional to the electroactive surface area (ESA) and is described by:[19]

$$C = C_\infty + Aexp\left(-\frac{WLT}{\upsilon_C}\right) \tag{2}$$

where C_∞ is the saturation capacitance, A is a negative constant, and υ_c is the critical volume of the PEDOT:PSS layer. When $WLT \ll \upsilon_C$, capacitance can be approximated as:

$$C \approx C_0 - A\frac{\upsilon}{\upsilon_c} \tag{3}$$

where $C_0 (= C_\infty + A)$ is the capacitance at zero volume, which is usually a small capacitance. At the limit of $C_0 \to 0$, $A \to -C_\infty$ thus leading the following inequality $|C_0| \ll |A|$. We note that the in case of $C_0 = 0$, Equation (3) gives the commonly used relationship for volumetric capacitance wherein $C^* = -\frac{A}{\upsilon_C}$.

Next, Equation (3) is used to calculate the current-voltage characteristics of an OECT, using the gradual channel approximation. For steady state DC conditions, the following equation is obtained that describes the output current of an OECT:

$$I_D = G\left(1 - \frac{V_G - \frac{V_D}{2}}{V_P}\right)V_D \tag{4}$$

where $G = \frac{q\mu p_0 WT}{L}$ is the conductance and V_p is the pinch off voltage, $V_p = qp_0/(C_0/\upsilon - A/\upsilon_c)$. The full derivation of Equation (4) is provided in the supplementary material. We note that Equation (4) has the form of the BM-model and indeed reduces to Equation (1) when $C_0 \to 0$ and $-\frac{A}{\upsilon_c} = C^*$. Moreover, Equation (4) implies that there are two saturation limits. First limit is current saturation due to de-doping which occurs when $V_D < V_G - V_P$. We define $V_D^{Sat} = V_G - V_P$ as the saturation voltage. Substituting it into Equation (4) gives:

$$I_D^{sat} = -G\frac{V_D^{sat2}}{2V_P} \tag{5}$$

The second saturation limit is when $\upsilon > \upsilon_c$. Here, $C = C_\infty$ which changes the pinch off voltage in Equation (4) to $V_P = \frac{\upsilon q p_0}{C_\infty}$.

Using Equation (4), the channel resistance, R_{ch}, of an OECT can be calculated. However, in the actual measurement, the total resistance, R_{tot} ($= V_D/I_D$) , of the device is measured, which is the channel resistance plus the contact resistance. Assuming that the contact resistance at the source and drain electrode are equal ($R_S = R_D = R_C$) then the total resistance of an OECT is obtained as:

$$R_{tot} = R_{ch} + R_S + R_D = \frac{L^2}{\mu\left[qp_0 WTL + \left(A\frac{WTL}{\upsilon_c} - C_0\right)\left(V_G - \frac{V_D}{2}\right)\right]} + 2 \cdot R_C \tag{6}$$

Equation (6) is non-linear L in sharp contrast to the linear L dependence as predicted from other OECT device models.

2.2. Experimental Validation of the NMC Model

To experimentally validate the model, numerous OECTs have been fabricated (125 individual devices), and their output characteristics have been obtained. The channel dimensions, both W and L of the OECTs systematically varied from 10, 20, 50, 100 to 200 µm. The thickness of the PEDOT:PSS layer was varied between 100 and 500 nm. The volume of the channel varied from 10 to 2×10^4 µm^3, which is well below the experimentally determined value for $\upsilon_c \sim 10^6$ µm^3.[19] Therefore, the condition outlined in Equation (3) is met and Equations (4) and (6) can be used for the analysis of the measured output curves. Equation (4) perfectly fits the output curve for all OECTs. A typical example is given in **Figure 2a**. It worth noting that the fits produced using NMC model, Equation (4), are qualitatively similar to those obtained from the BM model as indicated in Figure S1 (Supporting Information).

Following the fitting all OECT output curves using Equation (4), we obtained distributions of the fit parameters, namely p_0, μ, which account for the electronic properties and C_0, A, and υ_c, which describe the ionic properties of PEDOT:PSS. The results are summarized in Figure 2b–f for three different salt concentrations of 0.001, 0.01, and 0.1 M. The mean value of the hole densities p_0 is $7.48 \pm 0.21 \times 10^{20}$ cm^{-3} as shown in Figure 2b. The value of p_0 falls within the range of literature values of 3.1–15 $\times$ 10^{20} cm^{-3} for PEDOT:PSS layer.[30–32] The mean value of the hole mobility, Figure 2c, is 1.30 ± 0.86 cm^2 V^{-1} s^{-1}, which is within the range of value reported for PEDOT:PSS in literature, μ = 0.015–2.8 cm^2 V^{-1} s^{-1}.[30,31,33] In this respect the NMC mode gives values for hole concentration and mobility that are independent

© 2024 The Author(s). Advanced Electronic Materials published by Wiley-VCH GmbH

2199160x, 2024, 12, Downloaded from https://onlinelibrary.wiley.com/doi/10.1002/aelm.202400373 by MPI 355 Polymer Research, Wiley Online Library on [19/12/2024]. See the Terms and Conditions (https://onlinelibrary.wiley.com/terms-and-conditions) on Wiley Online Library for rules of use; OA articles are governed by the applicable Creative Commons License

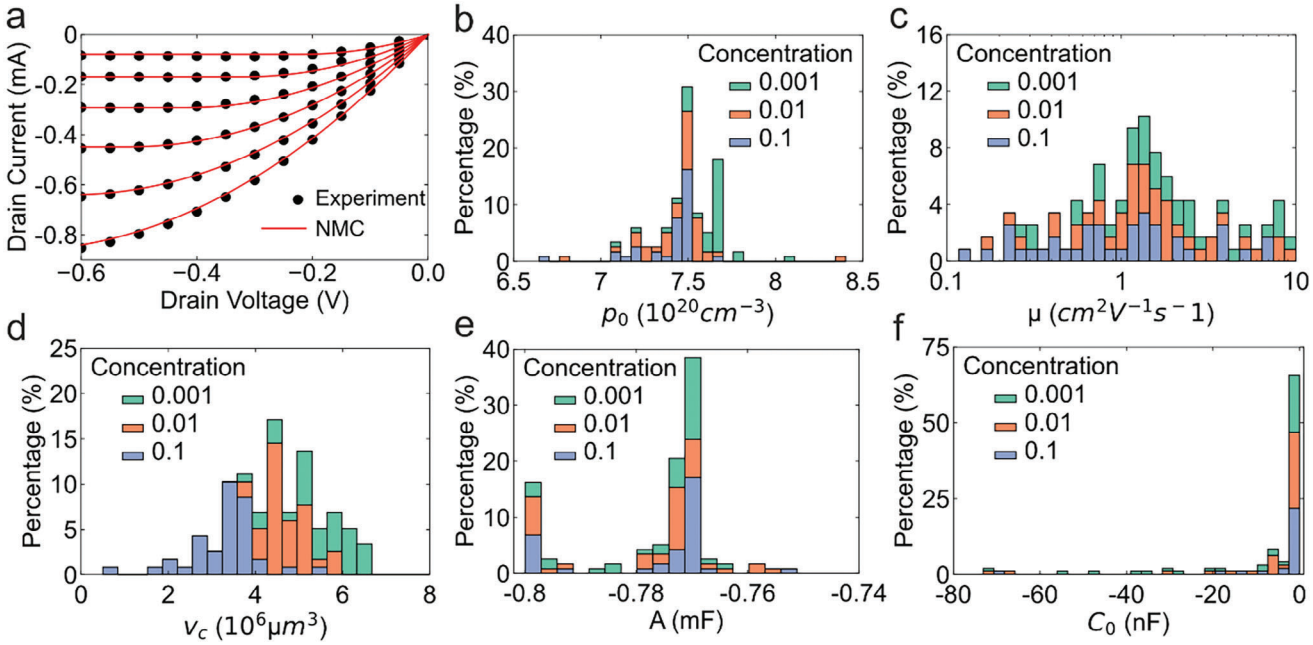

Figure 2. Validating NMC-model for OECTs. a) Output curve of an OECT device with channel width and length of 10 and 200 μm, respectively, with PEDOT:PSS thickness 500 nm, and electrolyte concentration 0.01 M. The graphs b–f) are the statistical distributions of the parameters of initial hole density, hole mobility, critical volume, capacitance exponential constant, and capacitance at zero volume, respectively, for varying electrolyte concentration. The different concentrations are stacked on top of each other.

of the electrolyte concentration, and follow a relatively normal distribution.

The NMC model also gives good estimates of the ionic properties of the PEDOT:PSS. The averages of the critical volume amounts to $v_c = 4.57 \pm 1.4\ 10^6\ \mu m^3$ (Figure 2d), which closely matches previously reported values of $4.6 \times 10^6\ \mu m^3$ obtained from impedance spectroscopy.[19] We note that V_c exhibits a very weak dependence on electrolyte salt concentration, as shown in Figure S2 (Supporting Information). The mean value for the constant A is -0.78 ± 0.01 mF (Figure 2e), which are again remarkably close to previously reported values of $A = -0.73$ mF.[19] The mean value for C_0 amounts to -8.01 ± 1.6 nF (Figure 2f), which agrees well with the prediction that C_0 should be very small approaching zero.[19] Histograms in Figure 2b–f include data for OECTs with different channel geometries, PEDOT:PSS layer thinness, and electrolyte salt concentrations. The values obtained for the electronic and ionic properties of the PEDOT:PSS layer closely matches those previously reported in the literature obtained using different techniques. It is therefore safe to say that the Equation (4) is self-consistent and can successfully be used to model OECTs.

2.3. Contact Resistance in OECTs

2.3.1. Thin PEDOT:PSS Films

To derive R_C, R_{tot} for transistors with a fixed W and various L is calculated. A typical resistance plot is given in **Figure** 3a for a fixed source drain bias for an OECT with a PEDOT:PSS layer thickness of 100 nm, and electrolyte salt concentration of 0.01 M. To estimate the contact resistance, Equation (6) is used to generate a line of best fit using values obtained in Figure 2 are used as the input. The y-intercept of the fit is $2 \times R_C$, as shown in Figure 3a. The NMC model accurately fits the experimental data ($r^2 = 0.998$) for all devices, and produces a positive value for the contact resistance that amounts to $376 \pm 67\ \Omega$. To demonstrate the strength of the NMC model, we have also employed TLM for the estimation of the contact resistance. As shown in Figure 3a, TLM produces a less accurate fit ($r^2 = 0.958$) and an unphysical negative contact resistance of $-485 \pm 134\ \Omega$. It is evident that the NMC model captures the non-linear dependence of R_{tot} versus L. The statistics of resistance analysis of the OECT devices using Equation (6) and TLM are given in Figure 3b. Equation (6) produces values that are positive with a normal distribution, with a mean of 376 Ω and standard error of 67 Ω. Strikingly, TLM analysis produces only unphysical negative contact resistances for all OECT devices in the series.

2.3.2. Thick PEDOT PSS Films

Next, R_C of OECTs with PEDOT:PSS layer thickness of 500 nm are analyzed using Equation (6) and TLM. Both methods produce positive R_C values. A typical analysis is shown Figure 3d. Both methods produce a fit with good quality that amount to $R^2 = 0.9998$ and 0.9953 for fits produced using Equation (6) and TLM, respectively. Contact resistance estimated by Equation (6) amounts to $48.9 \pm 4.7\ \Omega$ whereas TLM gives a value that is slightly smaller $34.1 \pm 3.3\ \Omega$. A histogram of R_C is given in Figure 3e. For R_C estimated with TLM, a more consistent picture emerges for thicker PEDOT:PSS films because a thicker PEDOT:PSS layer

© 2024 The Author(s). Advanced Electronic Materials published by Wiley-VCH GmbH

2199160x, 2024, 12, Downloaded from https://onlinelibrary.wiley.com/doi/10.1002/aelm.202400373 by MPI 355 Polymer Research, Wiley Online Library on [19/12/2024]. See the Terms and Conditions (https://onlinelibrary.wiley.com/terms-and-conditions) on Wiley Online Library for rules of use; OA articles are governed by the applicable Creative Commons License

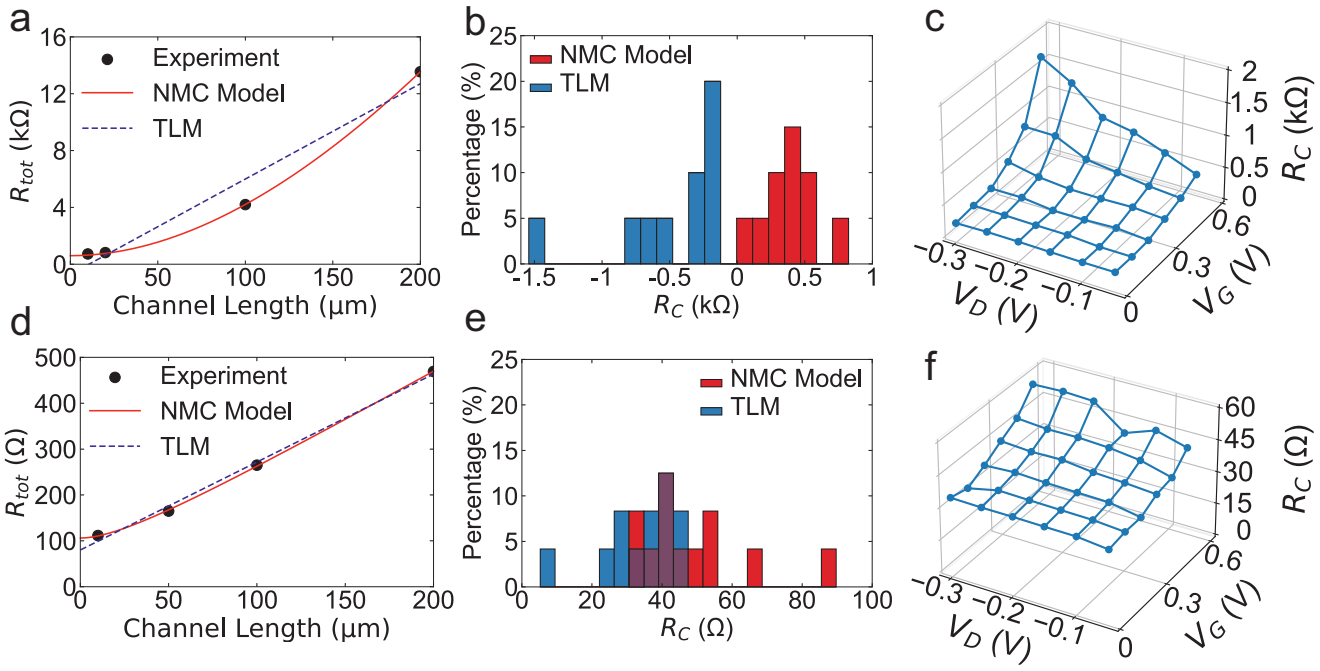

Figure 3. Contact resistance in OECTs. A typical resistance plot with representative fits was obtained from NMC model and TLM for an OECT with a) thin (100 nm) and d) thick (500 nm) PEDOT:PSS layer. Plots are for the operating conditions of V_G = 0.3 V and V_D = −0.1 V, for an OECT with a width of 20 μm and electrolyte concentration of 0.01 M. b,e) Histogram of estimated R_C for all channel widths and electrolyte concentrations. In the histograms the data sets are layered, therefore the purple represents where NMC model and TLM data overlaps. c,f) R_C versus V_D and V_G for 100 and 500 nm thick PEDOT:PSS devices, respectively. Devices had fixed width of 20 μm and electrolyte concentration of 0.01 M.

would mean that the effect of inhomogeneity is less pronounced. Nevertheless, the NMC model captures the non-linearity of the experimental R_{tot} versus L plot. It should be noted that the application of TLM consistently underestimates R_C. The differences in the estimated R_C of a single OECT is ≈20%. Relying on TLM results would adversely impact the estimated device performance (DC or AC), especially when upscaling into complex OECT-based integrated circuits. The results obtained using Equation (6) can lead to more reliable estimation of the performance of OECT-based circuits.

2.3.3. Voltage Dependence of R_C

Figure 3c,d show the voltage dependence of the contact resistance. It is observed that R_C shows a relatively weak gate (drain) voltage dependence at low drain (gate) biases. The voltage dependence of R_C becomes more pronounced as biases increase, where R_C shows almost a quadratic dependence on gate bias. At low gate biases, R_C does not show drain bias dependence, but at higher gate biases, a linear V_D dependence emerges.

2.3.4. Electrolyte Concentration Dependence of R_C

Having established the correct method for estimation of R_C, we investigate the effect of electrolyte concentration on contact resistance. A general trend is observed that the contact resistance increases with increasing the electrolyte salt concentration. The increase is more notable in thin devices than thick devices, as shown in Figure S3 (Supporting Information). We speculate that the trend could be due to enhanced Maxwell-Wagner effect at the contact interface that leads to a build-up of interfacial polarization that opposes the applied source-drain electric field, which manifested in the contact resistance. This explanation however is subject to further examination which is beyond the scope of the present study.

2.4. Transconductance and Design Guideline

According to Equation (4), transconductance is:

$$g_m = \frac{\partial I_D}{\partial V_G} = \frac{\mu WT}{L}\frac{A}{\upsilon_c}V_D - \frac{\mu C_0}{L^2}V_D \tag{7}$$

Transconductance is composed of two terms. For the case when $C_0 \to 0$, assuming that $-\frac{A}{\upsilon_c} = C^*$ Equation (7) reduces to the transconductance obtained from the conventional BM model. However, unlike the BM model, transconductance has $1/L$ and $1/L^2$ dependence. To validate Equation (7), transconductance for all OECTs was calculated from the transfer curves, and the maximum of transconductance is plotted in **Figure 4a** for devices with thick and thin PEDOT:PSS thicknesses, for electrolyte salt concentration of 0.01 M. Next, Equation (7) is employed to fit the g_m data. The NMC model fits the experimental data accurately with $r^2 = 0.968$ and $r^2 = 0.989$ for OECTs with thin and thick PEDOT:PSS layer, respectively. Next, we have inspected the behavior

© 2024 The Author(s). Advanced Electronic Materials published by Wiley-VCH GmbH

2199160x, 2024, 12, Downloaded from https://onlinelibrary.wiley.com/doi/10.1002/aelm.202400373 by MPI 355 Polymer Research, Wiley Online Library on [19/12/2024]. See the Terms and Conditions (https://onlinelibrary.wiley.com/terms-and-conditions) on Wiley Online Library for rules of use; OA articles are governed by the applicable Creative Commons License

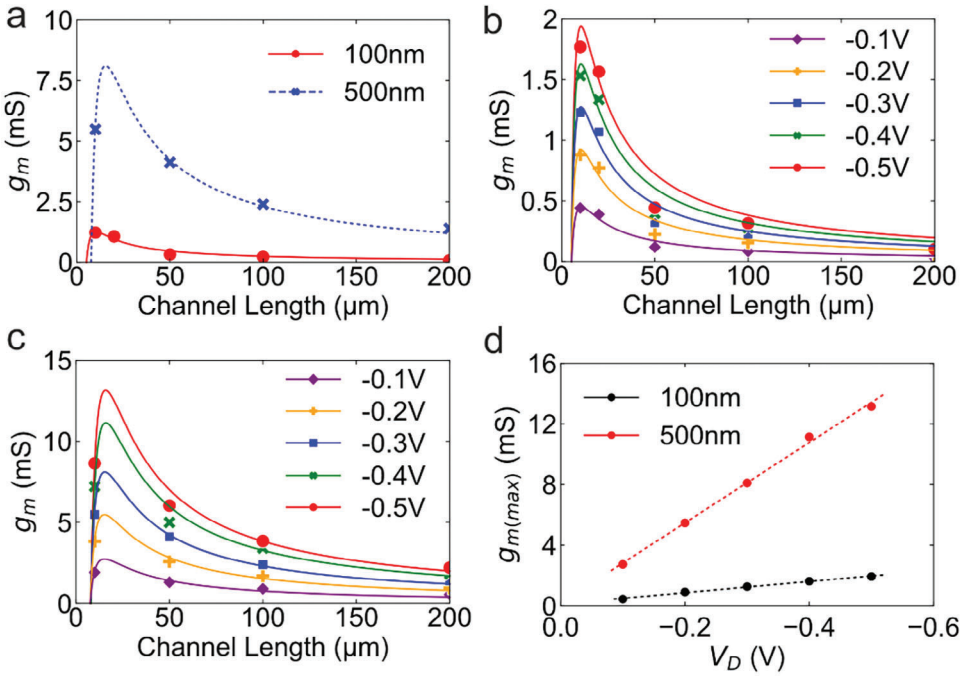

Figure 4. Transconductance versus channel length analysis. a) g_m versus L for OECTs with different PEDOT:PSS layer thicknesses at $V_D = -0.3$ V. b) and c) Dependence of transconductance on drain bias for an OECT with PEDOT:PSS thickness of 100 and 500 nm, respectively. For all the graphs symbols represent experimental data and lines represent the fitting of the NMC model. All devices had fixed $W = 20$ μm. d) Linear dependence of $g_{m(max)}$ on drain voltage, V_D, where for 100 and 500 nm. Data in parts a, b and c are for electrolyte salt concentration of 0.01 M.

of g_m at different source-drain voltages, Figure 4b,c for 100 and 500 nm PEDOT:PSS thicknesses, respectively. The NMC model accurately fits transconductance under various conditions. Interestingly, the fits show that g_m increases with reducing channel length as expected. However, at some channel length, g_m goes through a maximum and then reduces; a behavior that is more pronounced for OECTs with thicker PEDOT:PSS layer.

2.4.1. OECT Design Guideline

To better understand the behavior of g_m, we find the condition under which g_m is maximized ($\frac{dg_m}{dL} = 0$). The derivation would give the channel length for maximized g_m:

$$L_{max} = \frac{2C_0 \upsilon_c}{WTA} \tag{8}$$

Equation (8) correlates the device parameters, W and L, with the electrochemical characteristics of the semiconductor, C_0, υ_c, A, and can be used as a design criterion to fabricate OECTs with maximized transconductance. However, the prerequisite is to have prior knowledge of C_0, υ_c, A, the information that can be obtained simply by fabricating a capacitor with different semiconductor thicknesses and measuring the capacitance following the procedure suggested previously.[19]

By substituting Equation (8) into Equation (7), the maximum transconductance, $g_{m,max}$, is obtained:

$$g_{m,max} = \frac{\mu W^2 T^2 A^2}{4C_0 \upsilon_c^2} V_D \tag{9}$$

Equation (9) indicates that $g_{m,max}$ increases quadratically with the cross-sectional area, $W \times T$. Therefore, if OECTs with large transconductances are desired, the largest possible $W \times T$ should be used, and the channel length should be obtained from Equation (8). Note that larger $W \times T$ also has the benefit that minimises the contact resistance, as discussed earlier. We note that transconductance shows a very weak correlation with the electrolyte salt concentration, as shown in Figure 4b, which is in agreement with previous reports.[34] Finally, the linear dependence of transconductance on V_D is shown in Figure 4c,d, further indicating the internal consistency of the analysis of OECT data using Equation (4).

3. Conclusion

A new model that describes the DC current transport in OECTs has been developed that inherently takes inhomogeneities and non-monolithic capacitance of the PEDOT:PSS layer into account. The NMC model accurately and consistently fits the output and transfer curves of OECTs with varying geometrical dimensions, semiconductor layer thicknesses, and electrolyte concentrations.

It is demonstrated that TLM is invalid for PEDOT:PSS OECTs, particularly for thin film devices, when inhomogeneity of the PEDOT:PSS layer is more pronounced. For OECTs with thin PEDOT:PSS films TLM produces negative contact resistances and fails to capture the non-linear dependence of channel resistance versus length. The NMC model enables an accurate and consistent estimation of the contact resistance and provides a criteria to minimize the contact resistance.

© 2024 The Author(s). Advanced Electronic Materials published by Wiley-VCH GmbH

2199160x, 2024, 12, Downloaded from https://onlinelibrary.wiley.com/doi/10.1002/aelm.202400373 by MPI 355 Polymer Research, Wiley Online Library on [19/12/2024]. See the Terms and Conditions (https://onlinelibrary.wiley.com/terms-and-conditions) on Wiley Online Library for rules of use; OA articles are governed by the applicable Creative Commons License

Finally, a design guideline is presented and experimentally verifies that links the geometrical dimensions of the OECT with the electrochemical properties of the semiconductor. By elucidating the mechanism of capacitive coupling in OECTs, our model provides a guideline to optimize the device layout for specific bioelectronics operations in particular minimizing contact resistance and maximizing the transconductance, which are highly desirable for logic, neuromorphic and biosensing applications.

4. Experimental Section

Device Fabrication: The OCETs were fabricated using a previously reported standard microfabrication photolithography techniques.[35] Source, drain, and gate electrodes were patterned on. First, glass slides (26×76 mm^2) were cleaned in a soap (Micro-90) solution, and subsequently in a mixture of acetone:isopropanol with 1:1 (v/v) inside a sonication bath. Subsequently, the source and drain electrodes were patterned by photolithography (Süss MicroTec MA6) using photoresist (S1813), and gold (Au) electrodes (100 nm) with chromium (5 nm) as adhesion layer were sputter deposited using (Pfeiffer-vacuum sputtering system). Source and Drain electrodes were defined after the lift-off. Both channel length and width were systematically varied from 10, 20, 50, 100, and 200 µm. Next, the substrate was treated with Silane A-174 (gamma-methacryloxypropyltrimethoxysilane) which acts as an adhesion promoter for paralene-C, 2 µm thick, which was subsequently deposited. Before deposition of the sacrificial second paralyne-C, 2.5 µm thick, a soap solution (1% vol/vol) was drop casted, which act as an anti-adhesion agent during a subsequent peel-off step. A second photolithography step using AZ 9260 photoresist was performed to define openings in the photoresist in predetermined positions. Reactive Ion Etching (O_2/CF_4) was used to etch away the exposed parylene-C to access the OECTs' channels.

PEDOT:PSS with the following formulation of 38 mL PEDOT:PSS, 2 mL of ethylene glycol, 50 µL of 4-dodecylbenzenesufonic acid (DBSA), and 0.4 mL of (3-Glycidyloxypropyl)trimethoxysilane (GOPS) was spin coated on the substrate and a peel-off step removed the parylene-C sacrificial layer to define the transistors' channels. The spincoating speed was tuned to achieve PEDOT:PSS layers with thicknesses of 100 and 500 nm. Finally, the devices were hard baked at 140 °C for 1 h and placed in deionized water over night for the removal of the excess of low molecular weight molecules from the PEDOT:PSS film.

Device Characterization: All OECT measurements were performed with an aqueous NaCl electrolyte, at various concentrations of 0.001, 0.01, and 0.1 M. An Ag/AgCl electrode served as the gate electrode, and the *I–V* characteristics (both transfer and output) of the OECTs were obtained with a dual channel Keithley 2600 SMU.

Data Analysis: The experimental data were analyzed and fitted using "curve_fit", which was a built-in function part of the SciPy module in Python. The curve-fit used trust region reflective algorithm, which is a non-linear least squares method. The boundaries were defined for various parameters to avoid unphysical results such as negative carrier densities. First, the output curves of individual OECTs were fitted. The reported parameters in the literature were used as initial guesses for the hole mobility and density, and then varied to arrive at the best fit. The covariance of each parameter was used to calculate the error. Following obtaining all fit data, the distributions of all parameters were obtained. To obtain contact resistance values, the mean of the parameters obtained from fitting the output curves are used as the initial guess and were tuned within their standard deviation to obtain the curve of best fit for the resistance of the device. The same approach was used to fit the transconductance data.

Supporting Information

Supporting Information is available from the Wiley Online Library or from the author.

Acknowledgements

The authors wish to acknowledge technical assistance of C. Bauer, and H. J. Gutmann, and the financial support from the Max Planck Society, and the University of Bath. K.A. wishes to thank Garfield-Weston Foundation for the financial support.

Conflict of Interest

The authors declare no conflict of interest.

Data Availability Statement

The data that support the findings of this study are available from the corresponding author upon reasonable request.

Keywords

contact resistance, device model, OECT, organic electrochemical transistors, PEDOT:PSS, transconductance, volumetric capacitance

Received: May 13, 2024
Revised: October 22, 2024
Published online: November 9, 2024

[1] C. Z. Liao, C. H. Mak, M. Zhang, H. L. W. Chan, F. Yan, *Adv. Mater.* **2015**, *27*, 676.
[2] Y. J. Jo, K. Y. Kwon, Z. U. Khan, X. Crispin, T. I. Kim, *ACS Appl. Mater. Interfaces.* **2018**, *10*, 39083.
[3] P. Gkoupidenis, N. Schaefer, B. Garlan, G. G. Malliaras, *Adv. Mater.* **2015**, *27*, 7176.
[4] J. Rivnay, S. Inal, A. Salleo, R. M. Owens, M. Berggren, G. G. Malliaras, *Nat. Rev. Mater.* **2018**, *3*, 1.
[5] H. S. White, G. P. Kittlesen, M. S. Wrighton, *J. Am. Chem. Soc.* **1984**, *106*, 5375.
[6] S. T. Keene, T. P. van der Pol, D. Zakhidov, C. H. Weijtens, R. A. Janssen, A. Salleo, Y. van de Burgt, *Adv. Mater.* **2020**, *32*, 2000270.
[7] S. M. Kim, C. H. Kim, Y. Kim, N. Kim, W. J. Lee, E. H. Lee, D. Kim, S. Park, K. Lee, J. Rivnay, *Nat. Commun.* **2018**, *9*, 3858.
[8] D. Nilsson, M. Chen, T. Kugler, T. Remonen, M. Armgarth, M. Berggren, *Adv. Mater.* **2002**, *14*, 51.
[9] P. D'angelo, G. Tarabella, A. Romeo, S. L. Marasso, A. Verna, M. Cocuzza, C. Peruzzi, D. Vurro, S. Iannotta, *Materials* **2019**, *12*, 9.
[10] D. A. Bernards, G. G. Malliaras, *Adv. Funct. Mater.* **2007**, *17*, 3538.
[11] D. Ohayon, V. Druet, S. Inal, *Chem. Soc. Rev.* **2023**, *52*, 1001.
[12] P. R. Paudel, V. Kaphle, D. Dahal, R. K. Radha Krishnan, B. Lüssem, *Adv. Funct. Mater.* **2021**, *31*, 2004939.
[13] A. G. Polyravas, V. F. Curto, N. Schaefer, A. B. Calia, A. Guimera-Brunet, J. A. Garrido, G. G. Malliaras, *Flexible. Printed. Electron.* **2019**, *4*, 044003.
[14] A. F. Paterson, H. Faber, A. Savva, G. Nikiforidis, M. Gedda, T. C. Hidalgo, X. Chen, I. McCulloch, T. D. Anthopoulos, S. Inal, *Adv. Mater.* **2019**, *31*, 1902291.
[15] V. Kaphle, S. Liu, A. Al-Shadeedi, C. M. Keum, B. Lüssem, *Adv. Mater.* **2016**, *28*, 8766.
[16] J. T. Friedlein, J. Rivnay, D. H. Dunlap, I. McCulloch, S. E. Shaheen, R. R. McLeod, G. G. Malliaras, *Appl. Phys. Lett.* **2017**, *111*, 023301.
[17] G. Sych, P. Rannou, M. Jullien-Palletier, S. Sadki, Y. Bonnassieux, S. Sanaur, *Adv. Electron. Mater.* **2023**, *9*, 2201067.
[18] D. K. Shroeder, *Semiconductor Material and Device Characterization*, 3rd ed, John Wiley & Sons, Hoboken, New Jersey **2006**.

© 2024 The Author(s). Advanced Electronic Materials published by Wiley-VCH GmbH

2199160x, 2024, 12, Downloaded from https://onlinelibrary.wiley.com/doi/10.1002/aelm.202400373 by MPI 355 Polymer Research, Wiley Online Library on [19/12/2024]. See the Terms and Conditions (https://onlinelibrary.wiley.com/terms-and-conditions) on Wiley Online Library for rules of use; OA articles are governed by the applicable Creative Commons License

[19] M. Bianchi, S. Carli, M. Di Lauro, M. Prato, M. Murgia, L. Fadiga, F. Biscarini, *J. Mater. Chem. C* **2020**, *8*, 11252.
[20] M. Kemerink, S. Timpanaro, M. M. De Kok, E. A. Meulenkamp, F. J. Touwslager, *J. Phys. Chem. B* **2004**, *108*, 18820.
[21] A. V. Volkov, K. Wijeratne, E. Mitraka, U. Ali, D. Zhao, K. Tybrandt, J. W. Andreasen, M. Berggren, X. Crispin, I. V. Zozoulenko, *Adv. Funct. Mater.* **2017**, *27*, 1700329.
[22] S. M. Kim, C. H. Kim, Y. Kim, N. Kim, W. J. Lee, E. H. Lee, D. Kim, S. Park, K. Lee, J. Rivnay, M. H. Yoon, *Nat. Commun.* **2018**, *9*, 3858.
[23] J. Rivnay, P. Leleux, M. Ferro, M. Sasol, A. Williamson, D. A. Koutsouras, D. Khodagholy, M. Ramuz, X. Strakosas, R. M. Owens, *Sci. Adv.* **2015**, *1*, e1400251.
[24] D. A. Koutsouras, P. Gkoupidenis, C. Stolz, V. Subramanian, G. G. Malliaras, D. C. Martin, *ChemElectroChem* **2017**, *4*, 2321.
[25] J. Newman, W. Tiedemann, *AlChE J.* **2017**, *21*, 25.
[26] S. Carli, E. Busatto, S. Caramori, R. Boaretto, R. Argazzi, C. J. Timpson, C. A. Bignozzi, *J. Phys. Chem. C* **2013**, *117*, 5142.
[27] N. Kumar, R. T. Ginting, J. W. Kang, *Electrochim. Acta* **2013**, *270*, 37.
[28] C. M. Proctor, J. Rivnay, G. G. Malliaras, *J. Polym. Sci., Part B: Polym. Phys.* **2016**, *54*, 1433.
[29] J. T. Friedlein, R. R. McLeod, J. Rivnay, *Org. Electron.* **2018**, *63*, 398.
[30] F. Mariani, F. Conzuelo, T. Cramer, I. Gualandi, L. Possanzini, M. Tessarolo, B. Fraboni, W. Schuhmann, E. Scavetta, *Small* **2019**, *15*, 1902534.
[31] K. Nara, B. H. Lee, G. Kim, H. Kim, J. Kim, J. Lee, Y. H. Kahng, K. Lee, *Phys. Rev. Lett.* **2012**, *109*, 106405.
[32] D. A. Mengistie, C. Chen, K. M. Boopathi, F. W. Pranoto, L. Li, C. Chu, *ACS Appl. Mater. Interfaces.* **2015**, *7*, 94.
[33] V. Kostianovskii, B. Sanyoto, Y. Noh, *Org. Electron.* **2017**, *44*, 99.
[34] A. Savva, C. Cendra, A. Giugni, B. Torre, J. Surgailis, D. Ohayon, A. Giovannitti, I. McCulloch, E. Di Fabrizio, A. Salleo, *Chem. Mater.* **2019**, *31*, 927.
[35] D. A. Koutsouras, F. Torricelli, P. Gkoupidenis, P. W. M. Blom, *Adv. Mater. Technol.* **2021**, *6*, 2100732.

© 2024 The Author(s). Advanced Electronic Materials published by Wiley-VCH GmbH

2199160x, 2024, 12, Downloaded from https://onlinelibrary.wiley.com/doi/10.1002/aelm.202400373 by MPI 355 Polymer Research, Wiley Online Library on [19/12/2024]. See the Terms and Conditions (https://onlinelibrary.wiley.com/terms-and-conditions) on Wiley Online Library for rules of use; OA articles are governed by the applicable Creative Commons License